Designing Airgap-Stable Magnetic Linear Position Systems

Florian Slanovc[1,2,3], Dieter Suess[1], and Michael Ortner[2]

[1]Department of Physics of Functional Materials, University of Vienna, 1090 Vienna, Austria
[2]Silicon Austria Labs, 9524 Villach, Austria
[3]Vienna Doctoral School in Physics, University of Vienna, 1090 Vienna, Austria

This work addresses the topic of magnetic linear position detection, a common method used in modern industries to determine linear displacement by magnetic means. One major shortcoming of this method is the inherent airgap instability, which puts strong constraints on mechanical construction tolerances and limits resolution and sensitivity. We propose a method to improve the airgap stability by adding a second magnet, which makes the field and by extension the system output (locally) independent of the distance from the source. It is shown that the measurement error for 1-D systems can be reduced by a factor of ∼14 and for 2-D systems by a factor of ∼5 by application of this method for a realistic example.

Index Terms— **Airgap stability, field shaping, linear position, magnetic position detection, magnetic sensing.**

I. Introduction

MAGNETIC position and orientation detection systems determine the relative motion of mechanical parts. A permanent magnet is mounted on one part and a magnetic field sensor on the other, so that the relative motion can be calculated from the modulation of the magnetic field. In this way, depending on the requirements of the application, 1-D [1], [2], 2-D [3] translations, rotations [4]–[7] or even the combination of translation and rotation [8]–[10] can be measured. Such sensor systems are widely used in modern industrial applications due to their excellent properties in terms of cost, robustness, and non-contact. An overview to the variety of different types of magnetic sensors and their measuring methods is given in [11]–[14] and it is furthermore described for which applications they can be used in terms of field amplitudes [13], [14]. Sophisticated magnetic sensing ideas based on optical fibers with magnetic nanoparticles or flexible piezoelectric techniques have been explored in this context [15], [16]. With the clever implementation of one or more magnetic sensors, new opportunities are constantly opening up, such as magnet-based joysticks [10], space applications [17], geophysical studies on smartphone applications [18], permanent magnet motors [19] and have begun to replace existing mechanical, electronic and optical technologies. Today, there are more than 100 applications for magnetic position sensor systems in the automotive sector alone [20]–[22].

Magnetic linear position sensing is one common representative, with prominent applications like automotive shift forks, gas and brake pedals, detection of shifting shafts, flexible arms, lifting systems, in the gearbox, and many others. In this case, a permanent magnet moves along a straight line with a sensor mounted centrally above in a distance g termed the airgap. The range of the system is given by the stroke s with the magnet position $x \in [-s, s]$ [see Fig. 1(a)]. Such systems have been investigated, improved and optimized in the past in [23]–[26] by different sensor alignments and improved magnet shapes.

The magnetic field at the position of the sensor is given by $\mathbf{B}(x)$ and the sensor output $\boldsymbol{\beta}(\mathbf{B})$ is assumed to be proportional to it, $\boldsymbol{\beta} \propto \mathbf{B}$, which is characteristic for the commonly used linear Hall sensors. The system output signal $\zeta(\boldsymbol{\beta})$ is determined from the sensor output and the position is calculated from it

$$x \rightarrow \mathbf{B} \rightarrow \boldsymbol{\beta} \rightarrow \zeta \Rightarrow x. \tag{1}$$

For a typical linear position system, based on the magnet configuration from Fig. 1(c), the field $\mathbf{B}(x)$ is shown in Fig. 1(b) as a function of the position for a $12 \times 5 \times 5$ mm^3 magnet with magnetization $\mu_0 M = 1000$ mT and an airgap of $g = 5$ mm. Due to the symmetry, there are only two non-zero field components, $B_x(x)$ with even and $B_z(x)$ with odd behavior. While there are several other ways to choose magnet configurations [see Fig. 1(c)–(e)], in each case there is an even and an odd field component, B_{eve} and B_{odd}, on which the linear position sensing schemes rely.

If only a 1-D sensor is available, it must detect B_{odd} for a linear and unique relation between position and output

$$\zeta_{1\text{D}} = \beta_{\text{odd}}. \tag{2}$$

The potential range of such a system is then given by the central, monotonous linear part of the curve. A more sophisticated scheme can be used with a 2-D sensor

$$\zeta_{2\text{D}} = \text{atan}_2(\beta_{\text{odd}}, \beta_{\text{eve}}) \tag{3}$$

where atan_2 denotes the common two-argument arctangent function (see [25]). While the 2-D method features a higher level of signal stability, precision, and measurement range when compared to the 1-D counterpart, the latter is still used for its cost-efficiency. Any 1-D or 2-D sensor can be used to measure the field components [12], however, in industrial applications where moderate precision is sufficient, Hall-type sensors are a common choice [20].

Finally, a sensor system is characterized by its sensitivity S. It is given by the change of the system output with variation

Manuscript received 4 October 2021; revised 6 May 2022; accepted 30 June 2022. Date of publication 4 July 2022; date of current version 26 August 2022. Corresponding author: F. Slanovc (e-mail: florian.slanovc@silicon-austria.at).

Color versions of one or more figures in this article are available at https://doi.org/10.1109/TMAG.2022.3188474.

Digital Object Identifier 10.1109/TMAG.2022.3188474

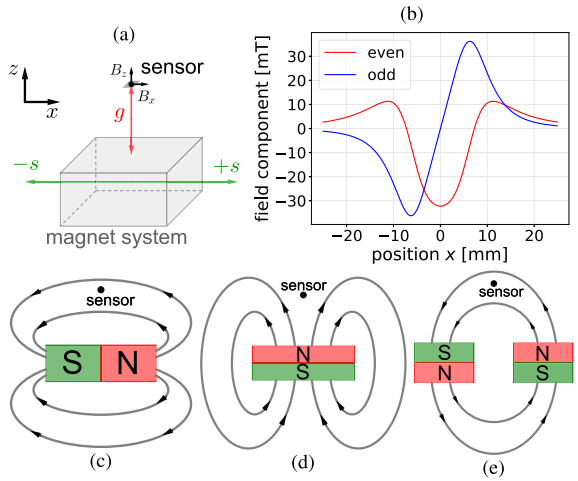

Fig. 1. In (a) moveable magnet system beneath a sensor is illustrated. It may consist of (c)–(e) different magnet assemblies, which all generate an even and an odd component of the magnetic field as shown in (b).

TABLE I

SYSTEM PARAMETER NAMES AND TYPICAL VALUES

parameter	symbol	unit	typical size
stroke	s	mm	5-20
position	x	mm	[-s,s]
airgap	g	mm	2-8
Magnetization	$\mu_0 M$	mT	200-1400
B-field	$\mathbf{B}$	mT	10-100
sensor output	β	V	0-5
sensitivity 1D	S	mT/mm	10-100 / s
sensitivity 2D	S	rad/mm	π / s
system output	ζ	-	-

of the observable (here magnet position x)

$$S(x_0, z_0) := \frac{\mathrm{d}\zeta}{\mathrm{d}x}(x_0, z_0). \tag{4}$$

A more detailed analysis of 1-D and 2-D sensing schemes, sensors, and systems can be found in [25] and [27]. In Table I below, we show a list of system parameters and their typical sizes for state-of-the-art Hall-based industrial linear position systems.

II. PROBLEM

Linear magnetic position sensor systems are currently used in many different applications and have been analyzed and improved in the past with respect to their functionality and cost optimization [23]–[27]. However, one of their major still unsolved problems is their inherent instability to airgap variations Δg. Industrial and automotive systems are only competitive if they are cost-efficient and fabrication tolerances are expensive to control. In automotive shift-fork systems airgap variations of up to $\pm 20\%$ are common. Such variations are usually calibrated out in an end-of-the-line process which ultimately results in large variations of the sensitivity. In addition, dynamic airgap variations of few percent over lifetime and during system operation must also be accounted for.

The sketch in Fig. 2 shows how an airgap variation leads to a inaccurate output signal $\zeta(x_0, z)$ instead of $\zeta(x_0, g)$, which further results in a wrong position estimation $\widetilde{x}_0$ for the real position x_0. In first order, the position error $\Delta x := x_0 - \widetilde{x}_0$, which results from airgap variation, is directly connected to the system output error $\Delta\zeta := \zeta(x_0, g) - \zeta(x_0, z)$ through the nominal sensitivity $S(x_0, g)$. We can therefore write

$$\Delta x(x_0, z) = \frac{\Delta\zeta(x_0, z)}{S(x_0, g)} \tag{5}$$

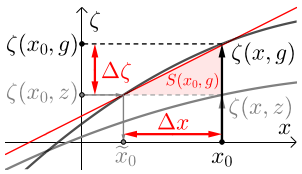

Fig. 2. Sketch of the system response. The airgap variation leads to a measurement error Δx, which is determined by $\Delta\zeta$ and the local slope $S(x_0, g)$ of the function $\zeta(x, g)$.

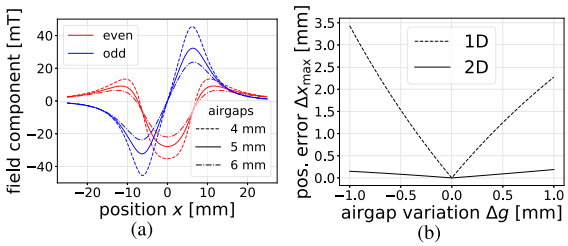

Fig. 3. (a) Airgap dependence of the field and (b) resulting position error $\Delta x_{\max}$ for 1-D and 2-D sensor schemes.

at position x_0. For convenience we have expressed everything through z, which is connected to the airgap variation through $z = g + \Delta g$. Clearly $\Delta x(x_0, g) = 0$ for all positions $x_0 \in [-s, s]$.

To demonstrate the effects of airgap variations, we show the magnetic field of the example system from Section I for different airgaps in Fig. 3(a). The maximal position error $\Delta x_{\max} := \max_{x_0 \in [-s,s]} \Delta x(x_0, z)$ as a function of the airgap variation Δg is given in Fig. 3(b) for $s = 5$ mm. The inherent higher stability of the 2-D scheme is clearly visible. The reason for this observation is that the system output signal of a 2-D sensor expression (3) contains the ratio of β_{odd} and β_{eve} and is independent of the amplitude of the measured magnetic field, which strongly depends on the airgap. However, since not only the amplitude but also the field angle varies as a function of the airgap, a small deviation remains in the 2-D system. In contrast, the output of the 1-D system (2) suffers drastically from the varying field amplitude.

III. PROPOSAL

To improve airgap stability in linear position systems, we propose to make the magnetic field $\mathbf{B}(x, z)$ or rather the system output $\zeta(x, z)$ locally independent of the airgap by combining the fields of several simple magnets in the spirit of [25], [28]. A sketch of the main idea is outlined in Fig. 4. There, the quick decay of the magnetic field of a small, close magnet is superposed with the slow decay of a large, distant magnet with reversed magnetization. By suitable arrangement of the two magnets (or magnet systems) we can achieve stationary points z_s of the field components in airgap direction, $\mathrm{d}\mathbf{B}/\mathrm{d}z(x, z_s) = 0$. Ideally, this is achieved for both components simultaneously and all positions x so that the system output becomes locally airgap independent

$$\frac{\mathrm{d}\zeta}{\mathrm{d}z}(x, z_s) = \frac{\mathrm{d}\zeta}{\mathrm{d}\mathbf{B}} \cdot \underbrace{\frac{\mathrm{d}\mathbf{B}}{\mathrm{d}z}(x, z_s)}_{=0} = 0. \tag{6}$$

The system output error is closely connected to the derivative of ζ in z-direction

$$\Delta\zeta(x, z) = \zeta(x, g) - \zeta(x, z) \simeq \frac{\mathrm{d}\zeta}{\mathrm{d}z}(x, z) \cdot \Delta g \tag{7}$$

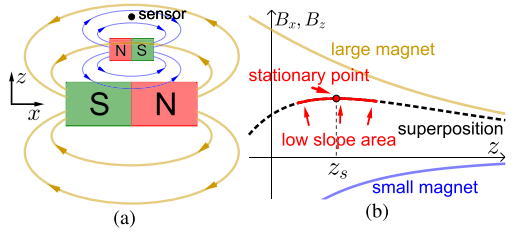

Fig. 4. (a) Antiparallel permanent magnet arrangement leads to (b) beneficial field superposition. For well-chosen dimensions, the sketch in (b) is approximately valid for both B_x and B_z and all x simultaneously (possibly with reversed sign).

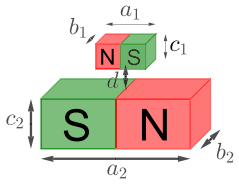

Fig. 5. Sketch of the magnet system variation parameters.

so that property (6) translates directly to the position error (5).

Note that stationary points of field **B** are sufficient, but in the 2-D case not necessary for the desired stationary points of the system output ζ. While it is difficult to achieve stationarity for all positions x at the same time, it is enough to sample the "low slope area" near z_s to improve stability [see Fig. 4(b)].

IV. Method

We compare 1-magnet (state-of-the-art) and 2-magnet (proposal) systems with 1-D and 2-D sensors, respectively. For good magnetic stability the 2-magnet system is constructed as indicated in Fig. 5 with magnet dimensions $a_1, b_1, c_1, a_2, b_2, c_2$ and distance d. This work is based on a multivariate optimization of these magnet system parameters to reduce the position error as much as possible. For comparison with optimal 1-magnet systems a similar optimization with $a_1 = b_1 = c_1 = 0$ is performed.

One must take care in the optimization process that the sensitivity does not tend to small or even negative values. This would violate the fundamental requirement that the system output ζ is a bijective map of the observable of interest.

A. Cost Function

The optimal system is found by global minimization of a cost function F which expresses the desired system qualities. We choose a weighted position error

$$\overline{\Delta x}(x_0) := \left(\int_{g-\Delta g}^{g+\Delta g} w(z) \cdot |\Delta x(x_0, z)|^2 \, \mathrm{d}z \right)^{1/2} \tag{8}$$

introducing the Gaussian weight function $w(z)$ with $\mu = g$ and $\sigma = \Delta g/3$ to account for realistic stochastic deviations of industrial systems. A corresponding cost function can then be defined as the maximal weighted position error over the whole range

$$F_p := \max_{x_0 \in [-s,s]} \overline{\Delta x}(x_0). \tag{9}$$

At the same time, the quality of a sensor system is strongly related to its sensitivity (4) which can be represented through another cost function F_s that could, for example, be given by the minimal sensitivity over the whole range. A total cost function F can then be written as a convex combination of these two terms, i.e.,

$$F := (1 - \lambda) F_p - \lambda F_s \tag{10}$$

with $\lambda \in [0, 1]$. Minimization of F leads to minimized position error and maximized sensitivity at the same time, where λ specifies the balance between F_p and F_s.

In this work, we set $\lambda = 0$ and neglect the sensitivity term F_s because the sensitivity must always be related to sensor resolution and noise behavior and we do not want to focus on one specific sensor type.

B. Scaling Invariance

A system where the sources are only ideal hard magnets is invariant with respect to the scaling of the spatial dimensions. This means that transformations of the form

$$(x, y, z) \longmapsto k_1 \cdot (x, y, z) \tag{11}$$

with $k_1 > 0$ on the whole system (i.e., stroke, airgap, magnet dimensions) result in the same magnetic field at the scaled sensor position. Furthermore, the scaling of the magnetization amplitude

$$M \longmapsto k_2 \cdot M \tag{12}$$

has no influence on the optimization problem, as the fields are directly proportional to it, $|\mathbf{B}| \propto M$.

The optimization is independent of the scaling, i.e., for different system sizes and materials the same optimum solution is found up to the scaling factor k_1 for geometric parameters and k_2 for field and magnetization. With (11) and (12) we can define a characteristic length l_0 and magnetic field M_0 and express all spatial variables, magnetizations and fields as dimensionless multiples of these parameters. Eventually, l_0 and M_0 can be used after solving the optimization problem, to set a system size and a material for practical applications.

C. Reasonable System Constraints

When dealing with realistic problems the end-user has specific requirements which must be included in the optimization process. These "reasonable system constraints" include:

1) the detection range or length of the stroke s;
2) the airgap g and airgap tolerance Δg;
3) a required resolution given by choice of sensor and sensitivity S;
4) the construction space with maximal magnet system dimensions $x_{\max}, y_{\max}, z_{\max}$ typically limited to $\sim s$;
5) the construction costs reflected in magnet volume V and magnetic material (magnetization M).

For our demonstration in Section V we choose $l_0 = 1$ mm, $\mu_0 M_0 = 1$ mT and a set of reasonable constraints in Table II that reflect standard system parameters for a linear position system.

D. Simulation Method

The fields are calculated by an analytical method using the magpylib package [29] which is based on the expressions from [30]–[32]. The speed of the analytical solution (effective sub-microsecond computation times) enables highly efficient multivariate parameter variation which is not feasible with

TABLE II

REALISTIC SYSTEM PARAMETERS AND CONSTRAINTS

s $[l_0]$	g $[l_0]$	Δg $[l_0]$	$x_{\max}$ $[l_0]$	$y_{\max}$ $[l_0]$	$z_{\max}$ $[l_0]$	V $[l_0^3]$	M_1 $[M_0]$	M_2 $[M_0]$
5	5	1	12	10	14	300	1000	1000

TABLE III

BOUNDS AND OPTIMIZATION RESULTS OF THE MAGNET SYSTEM PARAMETERS SHOWN IN FIG. 5

parameter	magnet 1			magnet 2		
	bound	1D	2D	bound	1D	2D
a_1	-	-	-	12	9.9	8.4
b_1	-	-	-	10	0.7	9.9
c_1	-	-	-	3	3.0	0.2
a_2	12	12.0	12.0	12	12.0	12.0
b_2	10	4.2	10.0	10	7.8	9.8
c_2	6	6.0	2.5	3	3.0	2.4
d	3	3.0	0.0	3	3.0	3.0

TABLE IV

SENSITIVITY $S(0, g)$ FOR ALL CONFIGURATIONS

	1-magnet		2-magnet	
	1D	2D	1D	2D
F_p	0.766 mm	0.042 mm	0.053 mm	0.009 mm
$S(0, g)$	3.39	0.26 rad/mm	0.65	0.19 rad/mm

common numerical methods like finite element (FE) or boundary element (BE). The error of the analytical solution is below 1% field amplitude and 1° angle for magnet L/D ratios of the order of 1 (cubical magnet dimensions) when compared to FE results of hard magnets with linear demagnetization slopes of $\mu_r < 1.05$ [10].

V. RESULTS

The optimization procedure described in Section IV is carried out to find optimal configurations for 1-D and 2-D systems with one or two magnets. Optimization bounds and results are given in Table III.

For each of the four cases, the resulting sensor output is shown in Fig. 6. Two effects can be observed there: On the positive side, the 2-magnet systems show increasing airgap stability confirming the original proposal. However, one has to pay for this stability with reduced field amplitudes and sensitivities. This is directly visible in the figures and is given quantitatively in Table IV.

In Fig. 7 we shown the actual position error of the sensor output Δx as a function of the position x and the airgap variation Δg. The lower level of position error within the working area (10 mm × 2 mm rectangle in the figure) is clearly visible.

Finally, we compare the weighted position error $\overline{\Delta x}(x_0)$ from (8) as well as the maximal position error $\Delta x(x_0, z)$ for $z \in [g - \Delta g, g + \Delta g]$ for all four configurations in Fig. 8(a) and (b). The 2-magnet systems are visibly improved over their 1-magnet counterparts.

VI. DISCUSSION AND OUTLOOK

In this article we show how to design an airgap stable linear position sensor system by adding a second magnet which stabilizes the field. Here stabilization means a reduction of the position error resulting from airgap variation. It was shown that the proposed method works for both, 1-D and 2-D sensor systems. For our model problem with airgap variation of

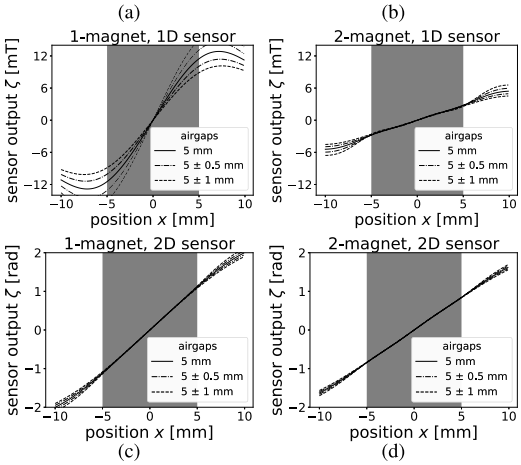

Fig. 6. Sensor output of optimum configuration in four different cases. (a) 1-magnet, 1-D sensor. (b) 2-magnet, 1-D sensor. (c) 1-magnet, 2-D sensor. (d) 2-magnet, 2-D sensor.

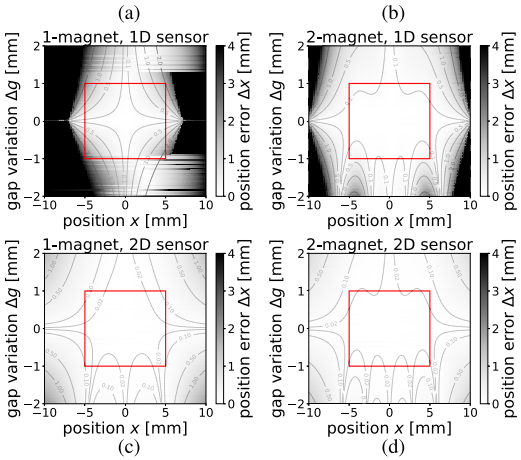

Fig. 7. Position error Δx for all four configurations. The red rectangle marks the working area ($\pm\Delta g$ airgap variation) of the sensor system. (a) 1-magnet, 1-D sensor. (b) 2-magnet, 1-D sensor. (c) 1-magnet, 2-D sensor. (d) 2-magnet, 2-D sensor.

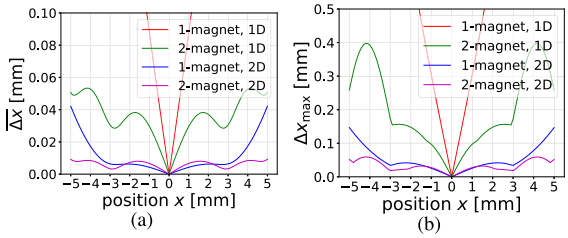

Fig. 8. Quantitative comparison of weighted position error $\overline{\Delta x}$ and maximal position error $\Delta x_{\max}$ of the four optimized systems with ranges of ±5 mm and airgap variations Δg of ±1 mm.

±1 mm, 5 mm nominal airgap and a range of 10 mm, this can lead to a reduction of the maximal weighted position error by a factor of ∼14 for 1-D systems and by a factor of ∼5 for 2-D systems within our chosen system requirements. It must be noted that these factors depend on the chosen system. Further improvements are possible which is also visible in Table III by the fact that the optimization returns boundary values. In general, we find that position error reduction by one order of magnitude in 1-D and a factor of 3–5 in 2-D is easily achieved for the typical linear position systems outlined in Table I.

The major downside of the proposed method is the reduction of field amplitude, which translates directly to the sensitivity and potential resolution. However, our results are just a proof of principle where we have demonstrated a novel airgap stabilization mechanism for magnetic systems. With additional constraints and the choice $\lambda > 0$ in (10), the balance between stability and field amplitudes can be adjusted at will.

While the proposed method is based on only two cuboid magnets, it is easily extended to more complex magnet structures as proposed in [25]. With the chosen spatial dimensions, we have investigated realistic size relationships in applications. Moreover, as mentioned in Section IV-B, the computation is scale invariant, so that other airgaps can be covered by simultaneously adjusting the magnet dimensions. The fundamental concept of stationary points in the magnetic field profile can of course be applied to other length ratios, magnet shapes, component alignments, etc. as well

Finally, we note that the odd component of a single magnet's field already has natural stationary points with a high level of airgap stability. However, these extrema lie very close to the magnet surface (assuming cuboids) so that if the system is scaled up to achieve desired airgaps, the magnet size exceeds our reasonable system constraints. Further investigation and exploitation of this effect is planned.

VII. Conclusion

Linear positioning systems are state of the art in many technical applications. Since they are mass-produced, the industrial requirements for them are mainly cost efficiency and robustness. With the idea of adding a small second magnet to the system, we could show that the common problem of airgap variation due to mechanical tolerances during installation can be massively reduced. Our approach shows how such a problem can be formulated, studied and solved as a mathematical optimization problem. The authors believe that potential further improvements to magnetic sensor systems can be studied in an analogous manner.

Acknowledgment

This work was supported in part by the COMET K1 Centre ASSIC Austrian Smart Systems Integration 100 Research Center and in part by the Vienna Doctoral School in Physics (VDSP). The COMET—Competence Centers for Excellent Technologies—Program is supported by BMVIT, 101 BMDW, and the federal provinces of Carinthia and Styria. The authors would like to thank Laura Ortner for review.

References

[1] D. S. Nyce, *Linear Position Sensors*. Hoboken, NJ, USA: Wiley, Nov. 2003.

[2] R. Wegener, F. Senicar, C. Junge, and S. Soter, "Low cost position sensor for permanent magnet linear drive," in *Proc. 7th Int. Conf. Power Electron. Drive Syst.*, Nov. 2007, pp. 1367–1371.

[3] U. Ausserlechner, A. Satz, and F. Gastinger, "Magnetic position sensors, systems and methods," U.S. Patent 8 717 010 B2, Infineon Technologies AG, Neubiberg, Germany, May 2014.

[4] G. Lemarquand and V. Lemarquand, "Annular magnet position sensor," *IEEE Trans. Magn.*, vol. 26, no. 5, pp. 2041–2043, Sep. 1990.

[5] J.-P. Yonnet, A. Foggia, and S. Adenot, "A differential magnetic position sensor," *Sens. Actuators A, Phys.*, vol. 81, pp. 340–342, Apr. 2000.

[6] L. A. Francis and K. Poletkin, *Magnetic Sensors and Devices*. New York, NY, USA: Taylor & Francis, Oct. 2017.

[7] S. Huber *et al.*, "A gradiometric magnetic sensor system for stray-field-immune rotary position sensing in harsh environment," *Proceedings*, vol. 2, no. 13, p. 809, Dec. 2018.

[8] S. Song *et al.*, "6-D magnetic localization and orientation method for an annular magnet based on a closed-form analytical model," *IEEE Trans. Magn.*, vol. 50, no. 9, pp. 1–11, Sep. 2014.

[9] D. Cichon, R. Psiuk, H. Brauer, and H. Topfer, "A Hall-sensor-based localization method with six degrees of freedom using unscented Kalman filter," *IEEE Sensors J.*, vol. 19, no. 7, pp. 2509–2516, Apr. 2019.

[10] P. Malagò *et al.*, "Magnetic position system design method applied to three-axis joystick motion tracking," *Sensors*, vol. 20, no. 23, p. 6873, Dec. 2020.

[11] J. E. Lenz, "A review of magnetic sensors," *Proc. IEEE*, vol. 78, no. 6, pp. 973–989, Jun. 1990.

[12] P. Ripka, *Magnetic Sensors and Magnetometers*. Norwood, MA, USA: Artech House, 2021.

[13] A. E. Mahdi, L. Panina, and D. Mapps, "Some new horizons in magnetic sensing: High-Tc SQUIDs, GMR and GMI materials," *Sens. Actuators A, Phys.*, vol. 105, no. 3, pp. 271–285, Aug. 2003.

[14] J. Lenz and A. S. Edelstein, "Magnetic sensors and their applications," *IEEE Sensors J.*, vol. 6, no. 3, pp. 631–649, Jun. 2006.

[15] A. Samavati *et al.*, "Magnetic field detection using a highly sensitive FBG probe," *Phys. Scripta*, vol. 95, no. 3, Feb. 2020, Art. no. 035509.

[16] Y. Zhao *et al.*, "Magnetic field sensor based on helical long-period fiber grating with a three-core optical fiber," *Opt. Exp.*, vol. 29, no. 13, p. 20649, Jun. 2021.

[17] M. Díaz-Michelena, "Small magnetic sensors for space applications," *Sensors*, vol. 9, no. 4, pp. 2271–2288, 2009.

[18] N. Campbell and E. Atekwana, "Evaluating the efficacy of magnetic sensors in smartphones for geophysical investigations," in *Proc. SEG Tech. Program Expanded Abstr.*, Aug. 2018, pp. 2582–2586.

[19] Y.-P. Yang and Y.-Y. Ting, "Improved angular displacement estimation based on Hall-effect sensors for driving a brushless permanent-magnet motor," *IEEE Trans. Ind. Electron.*, vol. 61, no. 1, pp. 504–511, Jan. 2014.

[20] *Xensiv Sensing the World*, Infineon Technologies AG, Neubiberg, Germany, 2019.

[21] C. P. O. Treutler, "Magnetic sensors for automotive applications," *Sens. Actuators A, Phys.*, vol. 91, nos. 1–2, pp. 2–6, Jun. 2001.

[22] J. P. Heremans, "Magnetic field sensors for magnetic position sensing in automotive applications," *MRS Proc.*, vol. 475, pp. 63–74, Dec. 1997.

[23] Y. Netzer, "A very linear noncontact displacement measurement with a Hall-element magnetic sensor," *Proc. IEEE*, vol. 69, no. 4, pp. 491–492, Apr. 1981.

[24] R. M. Grechishkin, L. E. Afanasieva, Y. G. Pastushenkov, and N. N. Maksimov, "Analysis of a linear position sensor with a Hall effect element," *Meas. Sci. Technol.*, vol. 5, no. 7, pp. 853–860, Jul. 1994.

[25] M. Ortner, "Improving magnetic linear position measurement by field shaping," in *Proc. 9th Int. Conf. Sens. Technol. (ICST)*, Dec. 2015, pp. 359–364.

[26] M. Ortner, C. Huber, N. Vollert, J. Pilz, and D. Suss, "Application of 3D-printed magnets for magnetic position detection systems," in *Proc. IEEE Sensors*, Oct. 2017, pp. 1–3.

[27] M. Ortner, M. Ribeiro, and D. Spitzer, "Absolute long-range linear position system with a single 3-D magnetic field sensor," *IEEE Trans. Magn.*, vol. 55, no. 1, pp. 1–4, Jan. 2019.

[28] A. Rahaman, "Contactless magnetic linear position sensor," U.S. Patenst 9 448 087 B2, Methode Electronics, Chicago, IL, USA, Sep. 2016.

[29] M. Ortner and L. G. C. Bandeira, "Magpylib: A free Python package for magnetic field computation," *SoftwareX*, vol. 11, Jan. 2020, Art. no. 100466.

[30] J. M. Camacho and V. Sosa, "Alternative method to calculate the magnetic field of permanent magnets with azimuthal symmetry," *Revista Mexicana de Física E*, vol. 59, no. 1, pp. 8–17, Jun. 2013.

[31] Z. J. Yang, T. H. Johansen, H. Bratsberg, G. Helgesen, and A. T. Skjeltorp, "Potential and force between a magnet and a bulk $Y_1Ba_2Cu_3O_7$-δ superconductor studied by a mechanical pendulum," *Superconductor Sci. Technol.*, vol. 3, no. 12, pp. 591–597, Dec. 1990.

[32] R. Engel-Herbert and T. Hesjedal, "Calculation of the magnetic stray field of a uniaxial magnetic domain," *J. Appl. Phys.*, vol. 97, no. 7, 2005, Art. no. 074504.